Atmos. Chem. Phys., 25, 11829–11845, 2025
https://doi.org/10.5194/acp-25-11829-2025

Atmospheric Chemistry and Physics
Open Access
EGU

Retention during freezing of raindrops – Part 2: Investigation of ambient organics from Beijing urban aerosol samples

Jackson Seymore[1], Martanda Gautam[1], Miklós Szakáll[1], Alexander Theis[2], Thorsten Hoffmann[2], Jialiang Ma[3], Lingli Zhou[4], and Alexander L. Vogel[3]

[1]Institute for Atmospheric Physics, Johannes Gutenberg University, Mainz, Germany
[2]Particle Chemistry Department, Max Planck Institute for Chemistry, Mainz, Germany
[3]Institute for Atmospheric and Environmental Sciences, Goethe University Frankfurt, Frankfurt, Germany
[4]South China Institute of Environmental Sciences, Ministry of Ecology and Environment, Guangzhou, China

Correspondence: Jackson Seymore (seymorej@uni-mainz.de)

Received: 13 December 2024 – Discussion started: 20 December 2024
Revised: 15 May 2025 – Accepted: 16 May 2025 – Published: 1 October 2025

Abstract. The freezing of hydrometeors causes certain water-soluble organic compounds dissolved in the supercooled cloud droplets to be released into the gas phase. This may lead to the vertical redistribution of substances that become available for atmospheric processes in the upper troposphere, such as new particle formation or ozone formation. Drop-freezing experiments were performed on the Mainz acoustic levitator (M-AL) using aqueous extracts of ambient samples of Beijing urban aerosol. The retention coefficients of over 450 compounds were determined. Most nitro-aromatics and organosulfates were fully retained, along with the aliphatic amines (AAs) and higher-order amines and amides, while the observed sulfides, lipids, aromatic hydrocarbons, and long-chain compounds are among the most unretained and, incidentally, are the fewest species present. The findings here also indicate that N- and S-containing compounds, primarily nitro and sulfate components of secondary organic aerosols (SOAs) anthropogenically related to NO_x and SO_2 chemistry, have enhanced retention, likely due to their increased polarity. An insignificant positive correlation between polarity and freezing retention, along with a significant negative correlation with vapor pressure and freezing retention, was observed. No sigmoidal relationship with the effective Henry's law constant was observed. This differs from the parameterizations of riming retention presented in the current literature, which is justified by the lower surface-to-volume ratio of the large drop size investigated. This study greatly expands upon the available experimental measurements of retention by investigating hundreds of compounds in complex chemical conditions that are more similar to the atmosphere than in previous literature studies.

1 Introduction

Atmospheric organic matter (OM) plays a critical role in climate regulation, both directly through radiation scattering and indirectly through cloud condensation nucleation, which impacts Earth's energy balance through radiative forcing (Fofie et al., 2018; Liu et al., 2018). These effects are controlled by factors such as their optical properties, size, and hygroscopicity (Dusek et al., 2006; Sun et al., 2021), which can change based on the proportions of primary organic aerosols (POAs) – directly emitted aerosols – and secondary organic aerosols (SOAs) – aerosols formed from the oxidation products of volatile organic compounds (VOCs) – and of inorganic constituents (Hallquist et al., 2009; Liu et al., 2021; Riva et al., 2019). Convective systems have been suggested to support new particle formation (NPF) in the outflow region by reducing existing particle concentrations, facilitating cold temperatures, and transporting reactive gases into regions with high actinic fluxes (Clarke et al., 1998; Zheng et al., 2021).

Nucleation-mode particles – with sizes in the lower tens of nanometers – have consistently been observed in concentrations of up to $10^4\,cm^{-3}$ from aircraft in the upper troposphere (Andreae et al., 2018; Casquero-Vera et al., 2020; Clarke et al., 1999; Heitto et al., 2024; Weigel et al., 2011; Williamson et al., 2019). These measurements significantly exceed the corresponding concentrations in the planetary boundary layer and indicate that the main source of such ultra-fine particles in the upper troposphere is in situ NPF rather than their direct transport from the boundary layer (Bardakov et al., 2021). The traditional explanation for this phenomenon has been that the reduction in existing aerosol particles in deep convective clouds eliminates removal processes for small particles and condensable vapors, supporting NPF (Clarke et al., 1998). However, Williamson et al. (2019) also showed that, even without these conditions, such as in tropical convection, these newly formed particles can still be found. They then argue that most models underestimate available organic matter at high altitudes and, as a result, predict less NPF in these regions. If this NPF is the result of an overlooked mechanism of organic matter transport, it is then critical to elucidate this mechanism for NPF precursors so as to constrain uncertainty around the influence of high-altitude NPF from convective outflows (Bardakov et al., 2021).

Publications by Borchers et al. (2024) and Jost et al. (2017) have demonstrated a potential mechanism for organic matter transport in mixed-phase clouds. They describe how organic compounds that are exchanged between the gas and aqueous phase in cloud droplets can either be trapped in the ice phase during freezing – washing them out by precipitation – or return to the gas phase by volatilization. This revolatilization caused by the freezing process leads to a vertical redistribution and has the potential to explain the occurrence of organic matter at high altitudes in regions with deep convection. Alternatively, earlier publications by Pruppacher and Klett (2010) and Snider and Huang (1998) suggested that complete sublimation of ice particles can also transport "retained" compounds trapped in the ice phase and release them at high altitudes.

In convective clouds, the main formation pathway of precipitation-sized ice particles is riming, i.e., the freezing of supercooled micrometer-sized cloud droplets on the surface of a millimeter-sized ice particle. Thus, riming retention is an important process for the vertical redistribution of water-soluble organic compounds (WSOCs). Convective clouds with warm bases favor the formation of millimeter-sized drops by collision–coalescence (Lamb and Verlinde, 2011), which can subsequently be uplifted in the updraft to regions with temperatures below 0 °C. Once beyond the freezing level, they can freeze and thereby release dissolved matter into the gas phase. This identifies freezing retention of millimeter-sized drops as a potential contributor to the vertical redistribution of WSOCs and was experimentally investigated in the present study.

The proportion of a substance that remains in the ice during this phase change is described by the retention coefficient R, which indicates the percentage of the trapped substance with a value between 0 and 1 (Bela et al., 2018; Iribarne and Pyshnov, 1990; Snider et al., 1992; Stuart and Jacobson, 2004). A species' retention is influenced by its chemical properties, such as its dimensionless effective Henry's law solubility constant (H^*), as well as the physical properties such as temperature, liquid-water content, droplet size, and ventilation. Substances with a small H^* are more likely to return to the gas phase during riming, which results in a lower retention coefficient. Additionally, these external and physical conditions of the droplet disproportionally influence the retention for these substances with a small H^* (Jost et al., 2017; Stuart and Jacobson, 2003, 2004).

Current experimental studies to determine retention coefficients for atmospheric constituents and relevant SOA precursors have focused on inorganic species, small organics, or single-component mixtures with significantly higher-than-natural concentrations. Additionally, current studies have only examined retention for cloud droplet sizes rather than for raindrop sizes. The few studies that look at complex mixtures are limited to compounds of similar families and only a handful of species (Borchers et al., 2024). Naturally occurring atmospheric constituents that are observed in rainwater are present as complex mixtures of potentially thousands of species (Seymore et al., 2023). To get closer to observing the retention of compounds in their natural conditions, this study presents measurements of retention coefficients for a real, complex mixture of WSOCs extracted from filter samples taken in an urban environment.

2 Methods

2.1 Sampling location and method

A high-volume sampler (HiVol) was run with quartz fiber TSP filters over 3 nights between 3 and 5 March 2022 in Beijing, China (40.0426° N, 116.4197° E), for an approximate sample volume of 550 m^3 between the hours of 21:00 to 09:00 CST (China standard time). These filters were sealed in aluminum foil and stored at −20 °C until analysis. Aqueous extracts of these filters were prepared by taking one-quarter of each filter, combining them (in total, three-quarters of a 203 × 254 mm filter area) in 30 mL Milli-Q water, and then extracting with an orbital shaker for 15 min. Multiple filters were used to produce the filter extract sample in order to ensure an adequate concentration and uniform background signal across multiple measurements. This also controls for potential differences in matrix effects from different filter compositions. The same extraction was performed for a blank sample; a total of three-quarters of unsampled filter area was extracted in 30 mL Milli-Q water for 15 min. These extracts were filtered through a 0.2 µm polytetrafluoroethylene (PTFE) filter; 10 mL of the prepared extract

was reserved for ultra-high-performance liquid chromatography high-resolution Orbitrap mass spectrometry (UHPLC-HRMS) analysis and stored at 3 °C, while the remaining 20 mL was sent to the Institute for Atmospheric Physics at the Johannes Gutenberg University of Mainz, Germany, for freezing experiments.

2.2 Mainz acoustic levitator (M-AL)

Freezing experiments were performed in an acoustic levitator (APOS BA 10, tec5 GmbH). This allows for contact-free single-drop levitation maintained by a standing ultrasonic wave. This setup and its relevant physical influences are described in detail by Diehl et al. (2014), Szakáll et al. (2021), and in Part 1 of this publication series by Gautam et al. (2025). For the freezing experiment, the M-AL is placed inside a walk-in cold room, where the ambient temperature was set to −15 °C. The M-AL is surrounded by a protective acrylic housing to prevent any disturbance from air motion which may cause unsteady temperature conditions, unstable levitation, or carry unwanted ice-nucleating particles onto the drop surface. Air temperature in the M-AL was measured by a PT100 sensor, and an infrared thermometer (KT 19.82 II, HEITRONICS) was used to monitor drop surface temperature.

The aqueous filter extract was injected with a syringe into the M-AL node to form a single free-floating drop with a diameter of 2 ± 0.1 mm. The drop was allowed to freeze without the introduction of an artificial-freezing nucleator. The freezing time was approximately 90 s on average but not longer than 3 min. Once the drop was fully frozen, it was removed from the M-AL and stored in a polytetrafluoroethylene (PTFE) vial at −20 °C until analysis. Enough drops to reach the minimum viable sample volume for analysis, 50 µL, were collected to produce a single sample (approximately 12 drops). A total of 30 drops were produced in total, which allowed for two full samples to be used for UHPLC-HRMS analysis. The blank filter extract was also used in the freezing experiment to produce two more travel blank samples for comparative analysis and background subtraction.

2.3 UHPLC-HRMS analysis

In addition to the M-AL frozen extract and the travel blanks, 100 µL of the reserved extract and Milli-Q solvent was analyzed by means of UHPLC-HRMS. Chromatographic separation was performed (Vanquish Flex, Thermo Fisher Scientific Inc.) on a reversed phase column (Cortecs Solid Core T3, 2.7 µm, 150 × 3 mm, with the corresponding VanGuard Cartridge, Waters Corp.). Samples were ionized in negative and positive mode using a heated electrospray ionization source (HESI-II Probe, Thermo Fisher Scientific Inc.) and then were detected with a high-resolution hybrid quadrupole–Orbitrap mass spectrometer (Q Exactive Focus, Thermo Fisher Scientific Inc.). The chromatographic settings and gradient are as follows: LC solvent A – ultrapure water with 0.1 % formic acid; LC solvent B – methanol with 0.1 % formic acid; flow rate – 400 µL min^{-1}; pre-column heater and post-column cooler – 40 °C; and gradient – 1 % B at 0 min, 1 % B at 1 min, 99 % B at 15 min, 99 % B at 16.5 min, 1 % B at 17.5 min, and 1 % B at 20 min. The MS settings were set at full-scan MS scan (m/z 50–750; resolution at 70 k), along with data-dependent MS2 in discovery mode (resolution at 17.5 k) for acquiring fragmentation spectra of the largest peaks.

2.4 Non-targeted analysis and property estimation

Compound identification confidence is communicated here using the convention described in Schymanski et al. (2014). The raw UHPLC-HRMS files were processed on Compound Discoverer 3.3 (Thermo Fisher Scientific Inc.). This software aligned chromatographic peaks of interest with a maximum shift of 0.1 min in retention time and a mass tolerance of ±2 ppm. Mass traces with retention times of less than 1.8 min were excluded as they are not considered to be chromatographically separated. Ions were detected if the peak intensity was at least 5×10^5 counts for $[M-H]^-$ for negative mode or for $[M+H]^+$ and $[M+Na]^+$ for positive mode. In addition to the mass-to-charge ratio of the detected ion, at least one corresponding isotopologue had to be measured. The tolerance between the measured and calculated intensity of the isotopologue was less than 30 %. These unknown compounds were then grouped with a retention time tolerance of 0.1 min to produce a merged MS feature, and those of them with a sample-to-blank ratio smaller than 5 were marked as background and were removed from the dataset. Any compounds that did not appear in the reserved sample of the filter extract were also removed from the dataset. A peak quality score was given on a scale of 0 to 10 – with 10 being a perfect chromatographic peak – for each mass trace based on its peak shape qualities, e.g., peak jaggedness or modality. For all mass traces with a peak quality higher than 6 in all samples, a predicted composition for each mass trace was calculated within ±2 ppm, with the allowed elements of carbon (C), hydrogen (H), nitrogen (N), oxygen (O), and sulfur (S). Compounds were grouped together as CHO, CHNO, CHOS, and CHNOS. It is important to note that phosphorus (P)-containing species were not considered for this study. All level-5 (L5) through level-1 (L1) compounds including any mass traces that did not fit a predicted composition within ±2 ppm were used for calculating retention coefficients using their integrated MS signals. Level-4 (L4) through L1 compounds with determined compositions were used for van Krevelen and Kroll analysis to highlight the validity of the dataset as a real, complex mixture of urban-influenced WSOCs. To aid in the visualization of MS data, a van Krevelen diagram cross-plots the H : C ratio as a function of the O : C ratio, while a Kroll diagram cross-plots the estimated average carbon oxidation state as a

function of the number of carbon atoms. An estimated vapor pressure at 298 K was then calculated for the elemental composition based on the parameterization by Li et al. (2016).

The predicted compound list was then matched against the mzCloud database (HighChem LLC, 2013–2021) for comparing MS^2 spectra. If a compound had at least one positive match with the predicted compound in the database, as well as a peak quality score above 8 in the reserved extract, this level-3 (L3) or stronger candidate was selected to be used for calculation of its effective Henry's law constant (K_H, mol Pa^{-1} m^{-3}). This was predicted using the HENRYWIN™ model as part of the EPI Suite™ package, which provides the values at 298 K (US EPA, 2024). If the EPI Suite™ was able to find an experimental value based on a CAS lookup match, those values were used over the model prediction. This is only applicable to the minority of identified species. The effective Henry's law solubility was converted to a dimensionless effective Henry's law constant (H^*) using the following equation:

$$H^* = K_H \cdot \bar{R}T, \tag{1}$$

where $\bar{R}$ is the ideal gas constant (8.3144626 m^3 Pa K^{-1} mol^{-1}), and T is temperature (K). This conversion allows for a dimensionless comparison and considers dissociation and hydration effects. This calculation, however, requires structural information about a compound. As a result, performing this calculation on an L3 tentative structural candidate can be specious or misleading. Regardless, H^* for structural isomers using HENRYWIN™ typically differs by less than 3 orders of magnitude, with an overall average of approximately 1.5 (Isaacman-VanWertz and Aumont, 2021). This accuracy is sufficient for this analysis.

2.5 Retention calculation and tracer corrections

The signals of species that also appeared in the travel blanks were first subtracted from the M-AL samples to remove their ambient signal but remained in the dataset as they exceeded the sample-to-blank ratio of 5 and could not be considered to be background. A naturally occurring tracer was selected from the dataset for both positive and negative mode to correct for any dilution, evaporation, and desorption that may occur. To be an ideal tracer, the compound should be fully retained during freezing and should have an adequate MS signal. For this work, the peak quality was required to be higher than 8 in the reserved extract and for there to be a positive database match for the predicted composition. For negative mode, this tracer was 4-nitrophenol ($C_6H_5NO_3$, m/z 139.0269, 9.7 min, L3). This was chosen as previous experiments by Borchers et al. (2024) have identified this compound to have a retention coefficient of 1.01 ± 0.07 during riming experiments, where desorption and evaporation effects are likely to be more influential than in the present experiment due to enhanced ventilation and much smaller droplet sizes. For positive mode, xylitol ($C_5H_{12}O_5$, m/z 152.0685, 1.6 min, L3) was selected as the tracer as its H^* has been determined to be higher than 10^8 (Compernolle and Müller, 2014), which, according to Borchers et al. (2024) and Jost et al. (2017), indicates that its retention coefficient can be safely assumed to be 1, even under the higher exchange conditions of wind tunnel experiments. Regardless of the accuracy of the L3-assigned structure, these tracers represent species with retentions very close to 1 that allow for a reference to that value to compare between samples and to make corrections for non-freezing mass exchange.

The equation for calculating the retention coefficient is adopted from Borchers et al. (2024) and Jost et al. (2017) and is used here as

$$R = \frac{S^{\text{sample}}_{\text{substance}} / S^{\text{RES}}_{\text{substance}}}{S^{\text{sample}}_{\text{tracer}} / S^{\text{RES}}_{\text{tracer}}}, \tag{2}$$

where the numerator describes the ratio between the peak area of the substance of interest in the ice sample ($S^{\text{sample}}_{\text{substance}}$) and in the reserved extract sample ($S^{\text{RES}}_{\text{substance}}$). The denominator describes the same ratio but for the tracer ($S^{\text{sample}}_{\text{tracer}} / S^{\text{RES}}_{\text{tracer}}$). Since no dilution effects are involved in the measurement and all samples are measured in the same aqueous matrix, signal ratios can be compared directly without a calibration curve, provided that the detector response is linear within the given range of measurements. Given that ions below the threshold intensity of linearity were excluded from the measurement, dynamic mass calibration of the HRMS was performed prior to measurement, and given that HRMS instruments of this generation show linear dynamic ranges of at least 5 orders of magnitude (Kaufmann and Walker, 2017), it is reasonable to assume linearity over the measurement range. As ventilation and evaporation effects are quite low in the M-AL (Szakáll et al., 2021), their effects are compensated for by the tracer. Compensating for desorption effects is more complex. As desorption is thought to be driven mainly by linear diffusion and thus enhanced by increased ventilation, species with higher-than-ambient concentrations, as well as species with higher vapor pressures, are thought to be disproportionally influenced. However, since the M-AL has little ventilation to enhance desorption, HiVol filter sampling is already biased against high-vapor-pressure species (Bidleman et al., 2020), and because ambient filter sampling is closer to ambient concentrations relative to previously simulated single-component mixtures, desorption effects are only compensated for by the tracer and nonuniform desorption effects are considered to be negligible.

Further data analysis was performed with MATLAB version R2023a. Distribution modeling was performed using the Distribution Fitter from the Statistics and Machine Learning Toolbox 12.5 based on the Stable Distribution and *t* Location-Scale Distribution models provided in *Univariate Stable Distributions* (2020) and *Univariate Continuous Distributions* (2015) (Nolan, 2020; Yee, 2015).

3 Results and discussion

3.1 Dataset description

In the negative mode, from over 2800 MS features measured, 548 significant, non-background-detected compounds were found. A total of 208 met the peak quality constraints and were then used for analysis. A total of 196 compounds (94 %) had successfully assigned compositions, and 77 were then selected for additional property calculations.

In the positive mode, 342 significant, non-background-detected compounds were found from over 1800 features. A total of 250 met the peak quality constraints and were then used for analysis. A total of 218 of those compounds (87 %) had successfully assigned compositions, and 84 were then selected for additional property calculations. Comparatively fewer compounds were assigned compositions in the positive mode as phosphorous-containing species were not considered. Phosphorous-containing species can represent almost one-third of positively ionizable species in rainwater WSOCs (Seymore et al., 2023), and so these species are likely to make up a significant portion of species variety that is not considered.

Figure 1 illustrates that the dataset is indicative of a typical urban-influenced WSOC profile of a dilute sample. In the negative mode, the most significant signals are several nitrophenols and nitro-aromatics; notably, $C_6H_5NO_3$ (m/z 139, 9.7 min, L3) and $C_6H_4N_2O_5$ (m/z 184, 10.3 min, L3) are tentatively identified as 4-nitrophenol and 2,4-dinitrophenol, respectively. These nitrophenols ionize efficiently in (−)HESI, which explains, in part, their prominence in Fig. 1b, where they cluster around 0.6–0.9 H/C and are indications of biomass- and fossil-fuel-burning emissions (Taneda et al., 2004). The prominent CHOS compounds in the negative mode are alkylorganosulfates, notably $C_5H_{12}O_4S$ (m/z 168, 8.4 min, L3) and $C_8H_{18}O_4S$ (m/z 210, 12.9 min, L3), which are typical markers of secondary processed automobile- and shipping-traffic OM (Blair et al., 2017; Qi et al., 2021). These can be seen most easily in Fig. 1b above 2 H/C. Some of the other notable CHOS compounds below 2 H/C are terpene-derived organosulfates in addition to compounds such as camphorsulfonic acid ($C_{10}H_{16}O_4S$, m/z 232, 9.4 min, L2), which also demonstrate secondary processing with sulfate aerosols (Iinuma et al., 2007; Surratt et al., 2007).

The most significant positive-mode signals in Fig. 1 come from caprolactam ($C_6H_{11}NO$, m/z 114, 7.0 min, L2) and several coumarin derivatives ($C_9H_6O_2$, m/z 146, 7.4 min, L2; $C_9H_8O_4$, m/z 162, 10.9 min, L3; $C_9H_8O_3$, m/z 164, 8.7 min, L3; $C_{10}H_8O_4$, m/z 192, 9.0 min, L3). Caprolactam is a cyclic amide and is indicative of industrial emission influence as it is primarily used for manufacturing synthetic fibers but is also used in numerous other manufacturing activities. Caprolactam is a monitored compound on the hazardous air pollutants list by the United States Environmental Protection Agency (US EPA, 2020). Coumarin species are known brown-carbon components and have biomass burning sources, as well as potential secondary pathways (Xing et al., 2023).

The several other prominent CHNO compounds are mostly amines, e.g., $C_{11}H_{23}NO_2$ (m/z 201, 3.6 min, L3), $C_9H_{11}NO_2$ (m/z 165, 3.7 min, L3), and DL-Stachydrine ($C_7H_{13}NO_2$, m/z 143, 1.8 min, L2). This is consistent with known amine–nitrate aerosol formation during winter months, where there are sources of amine salts and semi-volatile organic amine compounds, particularly in areas with high agricultural and combustion emissions (Price et al., 2016). The other prominent CHNO compounds are tentatively identified as amides such as $C_{12}H_{18}N_2O$ (m/z 206, 6.6 min, L3), $C_{10}H_{14}N_2O$ (m/z 178, 4.2 min, L4), and $C_3H_4N_4O_2$ (m/z 128, 1.8 min, L3), which can be further secondary products of AA (Price et al., 2014) or the result of anthropogenic emissions (Li et al., 2022; Schollée et al., 2017). These amine and amides tend to have lower retention times and can been seen in the lower cluster in Fig. 1a. The CHO species present are generally either aromatics or aliphatic acids and are separated out as such in the van Krevelen diagram in Fig. 1b, with aromatics below 1.5 H/C and acids above 1.5 H/C, such as $C_{12}H_{24}O_3$ (m/z 216, 14.2 min, L3) and $C_9H_{10}O_3$ (m/z 166, 9.1 min, L3). Very few biogenic CHO species are present as there are very few CHO species within 1.5–1.8 H/C that would indicate humics, ligins, or other raw biomass markers (Qian et al., 2013). This is consistent with the winter season sampling (Ma et al., 2022). Further characterization of the nonaromatic CHO is difficult to generalize as there are a variety of sugars, ethers, alcohols, and acids that represent various possible biogenic species, terpenoids, and terpene derivatives. For example, xylitol (possibly arabitol) ($C_5H_{12}O_5$, m/z 152, 1.6 min, L3), hexitol ($C_6H_{14}O_6$, m/z 182, 1.6 min, L3), cinnamic acid ($C_9H_8O_2$, m/z 148, 8.7 min, L3), phthalates such as dimethyl phthalate ($C_{10}H_{10}O_4$, m/z 194, 10.9 min, L2) and phthalic acid ($C_8H_6O_4$, m/z 166, 7.6 min, L3), succinic acid ($C_4H_2O_3$, m/z 98, 2.6 min, L3), levoglucosan ($C_6H_{10}O_5$, m/z 162, 4.5 min, L2), and farnesol ($C_{15}H_{26}O$, m/z 222, 14.6 min, L3) are all species potentially identified in the dataset.

A few CH and CHN compounds were found only in the positive mode, primarily AA and a couple of aromatic hydrocarbons. Combined, these represent less than 11 % of the positive-mode compounds. Only one CHS species was identified ($C_{18}H_{12}S$, m/z 260, 10.0 min, L4) but was not used for analysis as it was below peak quality requirements. No CH, CHN, or CHS species were found in the negative mode.

3.2 Retention coefficients

The histograms presented in Figs. 2 and 3 illustrate the distribution of retention coefficients determined for this dataset. Each histogram shows a peak at 0.96, 0.93, and 0.94 for (−)HESI, (+)HESI, and the full dataset, respectively, with

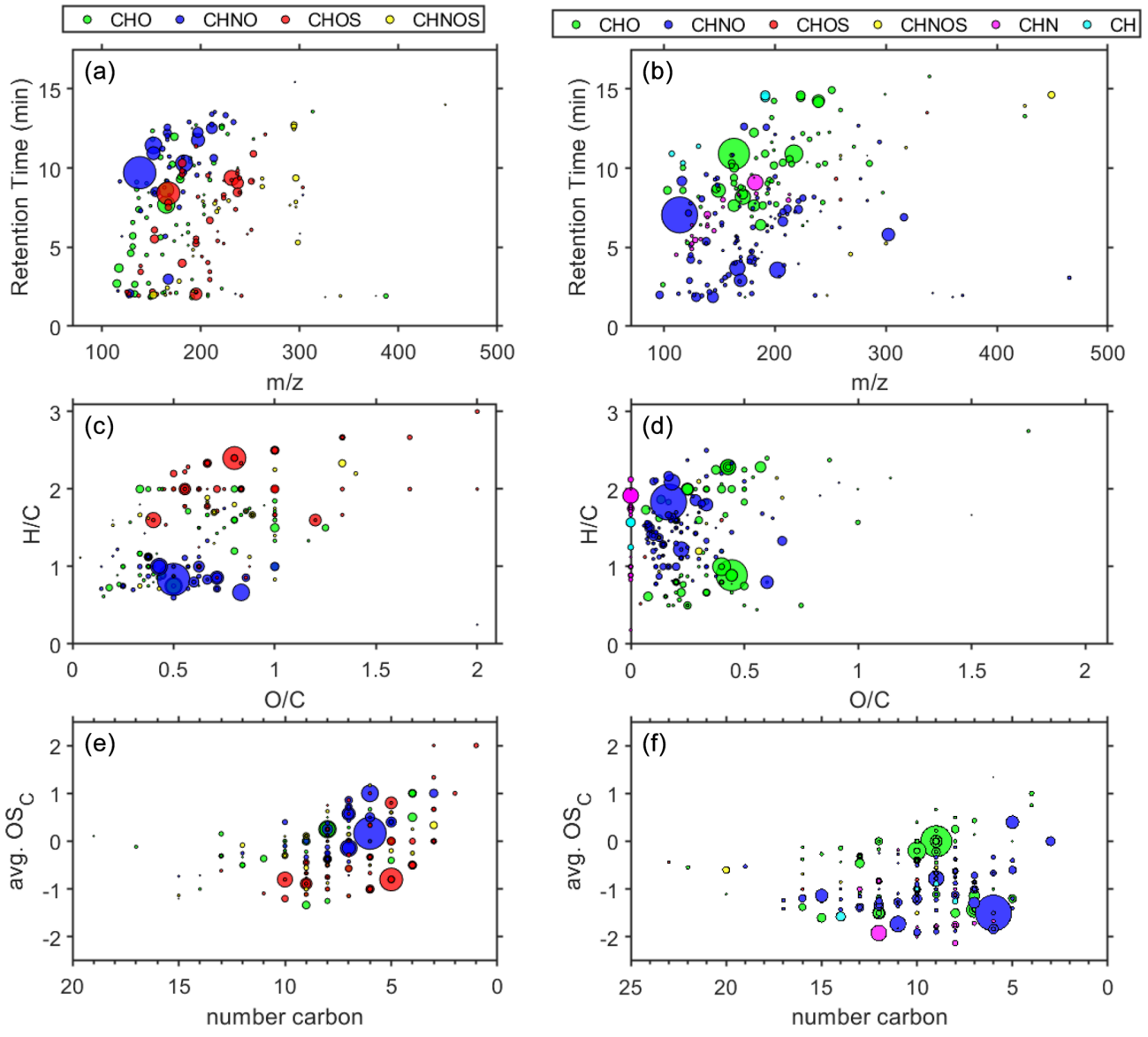

Figure 1. **(a)** Scatterplot of HPLC retention time (min) vs. m/z ratio; **(b)** van Krevelen diagram of O/C ratio vs. H/C ratio; **(c)** Kroll diagram of number of C atoms against the average oxidation state of C. Panels **(a)**, **(c)**, and **(e)** are for negative ionization mode or (−)HESI, while panels **(b)**, **(d)**, and **(f)** are for positive ionization mode or (+)HESI. The area of the marker indicates relative intensity in the reserved extract, while color denotes the compositional class of the assigned compound: green for CHO, blue for CHNO, red for CHOS, yellow for CHNOS, magenta for CHN, and cyan for CH.

average retentions at 0.95 and with standard deviations of 0.21 and 0.53. These values and the values for each compound class are presented in Table 1. Visually, the distributions in Fig. 2 appear to be non-normal, suggesting that a true distribution is being measured. Additionally, Fig. 4 shows that the data deviate strongly from a normal distribution. Both Shapiro–Wilk and Shapiro–Francia tests indicate nonnormality (p values of 0.4052 and 0.3940 for (−)HESI and 0.5698 and 0.5611 for (+)HESI).

Combining these distributions and filtering out outliers, the dataset is fitted with two distributions to model the dataset: Stable and t Location-Scale. The parameters for these fits can be found in Tables S1 and S2 in the Supplement. These distributions are functional estimations of the statistical density of retention coefficients based on the empirical measurements in this experiment. The Stable Distribution appears to model the data most accurately as the parameter errors are lower than the t Location-Scale Distribution, and the data points in Fig. 4 lie closer to the Stable Distribution curve.

The means of the composition classes in (−)HESI range between 0.90 and 0.99, with an unweighted average of 0.95

Table 1. Mean and median retention coefficients by compound class and heteroatom group.

	(−)HESI					(+)HESI				
	Mean	σ	Median	n	n %	Mean	σ	Median	n	n %
Total	0.95	0.21	0.96	208	100	0.95	0.53	0.93	250	100
CHO	0.90	0.25	0.91	68	32.7	1.01	0.82	0.90	73	29.2
CHN	–	–	–	–	–	1.07	0.21	1.04	22	8.8
CHNO	0.96	0.08	0.95	46	22.1	0.94	0.21	0.93	108	43.2
CHNOS	0.97	0.23	0.98	26	12.5	1.11	0.34	0.99	7	2.8
CHOS	0.99	0.23	0.98	56	26.9	0.67	0.59	0.99	3	1.2
CH	–	–	–	–	–	0.66	0.55	0.78	5	2.0
O containing	0.95	0.21	0.96	196	94.2	0.97	0.54	0.92	191	76.4
N containing	0.96	0.15	0.96	73	35.1	0.97	0.22	0.95	137	54.8
S containing	0.99	0.23	0.98	83	39.9	0.98	0.44	0.99	10	4.0

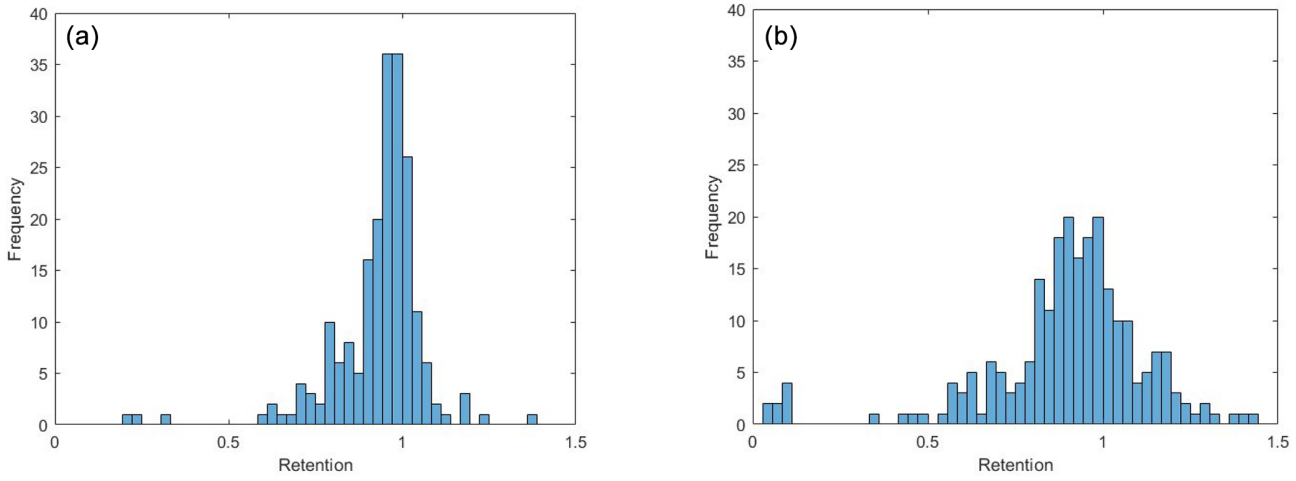

Figure 2. Histograms of retention coefficients for all measured L5 and above compounds that met peak quality constraints. **(a)** (−)HESI. **(b)** (+)HESI.

and a standard deviation of 3 %. In contrast, the means of the composition classes in (+)HESI vary more, by up to 40 %. The deviations and ranges of values are also wider in (+)HESI, from 0.21 to 0.82, as seen in Table 1. Visually, this can be seen in Fig. 5. For both ionizations, CHNOS tends to be the highest retained, along with CHN in (+)HESI. These CHNOS compounds have some of the highest molecular masses in the dataset, as is evident in Fig. 1. The CHN species present are all AA. In (+)HESI, CHNOS, CHOS, and CH represent the smallest portion of the dataset – less than 6 % – and some of the most variably retained species. For CH, this follows with the variability in hydrocarbon aqueous solubility; however, this variability is more likely to be explained for CHNOS and CHOS with the smaller sample set bias. Notably, with lower median retentions in both ionizations, most CHO compounds have lower retentions than CHNO compounds. In (−)HESI, CHNO is mostly nitro-aromatics, while, in (+)HESI, CHNO is mostly amines and amides. CHO represents a more similar distribution of organic acids and terpenoids in both positive and negative mode, with more nonpolar species represented in (+)HESI. The lower retention among CHO may then be based on its distribution of organic acids versus terpenoids. These data suggest that nitrate species and amines and/or amides have similar retentions. It is known that NO_x participates in the reversible and irreversible uptake of isoprene to aerosol liquid water and can further react with isoprene to produce a substantial number of organonitrates (El-Sayed et al., 2018; Tsiligiannis et al., 2022). While it is also known that organic nitrogen represents an important fraction of WSOCs (Saxena and Hildemann, 1996; Zhang et al., 2002), these data may also indicate that nitrogen chemistry on CHO species enhances their retention in hydrometeors. Other UHRMS studies of rainwater have suggested similar explanations for nitrogen uptake in hydrometeors and for rainwater organic nitrogen's high bioavailability (Seymore et al., 2023).

The distributions of CHNO and CHOS in (−)HESI seen in Fig. 6 show a coincidence of the mean and median, along

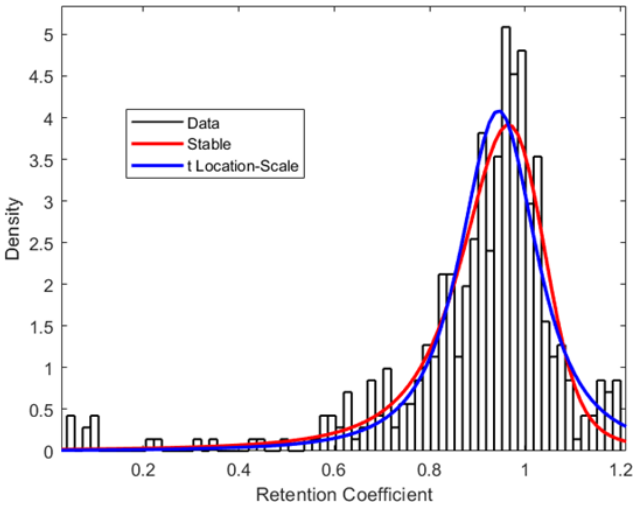

Figure 3. Merged histogram for (−)HESI and (+)HESI of all retention coefficient measured fits with Stable and t Location-Scale Distribution parameterizations of statistical density.

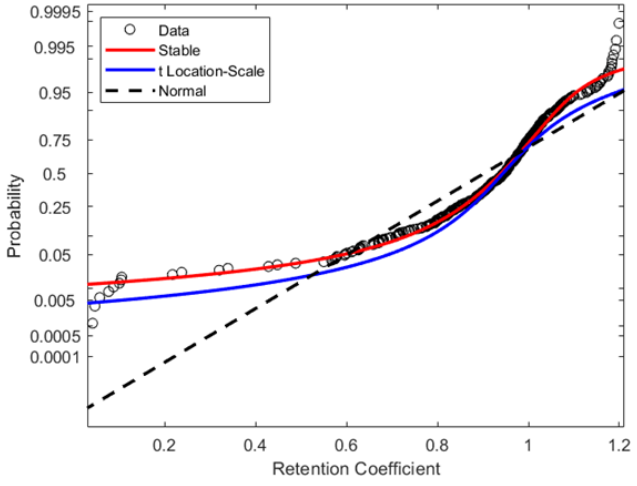

Figure 4. Probability plot of retention coefficients with the Stable and t Location-Scale Distribution parameterizations and a normal distribution.

with strong symmetry around the mean. This indicates visually that they appear to be normally distributed, suggesting that the true retentions for the whole of these compound classes may be close to 1. Both the Shapiro–Wilk and Shapiro–Francia tests indicate normality (p values: 0.1920, 0.1922) for CHNO but not for CHOS (7.7595×10^{-9}). It would therefore be reasonable to assume a normal distribution for CHNO, but CHOS cannot be rigorously stated to be normally distributed. CHO and CHNOS show unique distributions, with a significant number of values within $-\sigma$ and below, indicating that there are certain CHO species that are not retained during freezing.

For (+)HESI, the samples sizes for CHNOS, CHOS, and CH are too small to make meaningful descriptions of their distributions. For CHO, CHN, and CHNO, the distributions are visually non-normal and also do not pass any statistical test for normality. The distributions also appear to be less smooth than their negative-mode counterparts, likely a result of previously discussed ionization variability in (+)HESI. Notably, (+)HESI shows a few species with very low retention, specifically within the CHO, CHOS, and CH groups. Specifically, these are $C_{14}H_{22}$ (m/z 190, 14.5 min, L3), $C_{15}H_{26}O$ (m/z 222, 14.6 min, L3), and what appears to be a phenyl-sulfide species ($C_{16}H_{18}OS$, m/z 258, 8.0 min, L4). This is the only identified organosulfide within the dataset. It would be speculative to say that its low retention may indicate that organosulfides as a class are unretained and thus are unlikely to appear in the dataset. Its low retention likely has more to do with its low polarity. $C_{14}H_{22}$ and $C_{15}H_{26}O$ as long-chain, nonpolar species demonstrate that species with lower aqueous solubilities are also likely to have low retentions.

Concerning heteroatoms, the distributions and ranges of retentions are quite similar among all groups. Oxygen-containing species appear to have a slightly wider distribution, which is mostly weighted by the CHO class. Nitrogen-containing species have a smaller standard deviation than the O- or S-containing species, indicating fewer species with variable retentions and more fully retained compounds. This further suggests that nitrogen inclusion enhances retention (see also Fig. S1).

3.3 Correlation of retention coefficients with chemical properties

Figure 7 shows linear regressions for retention coefficients with HPLC retention time. With reverse-phase HPLC, retention time is a direct proxy for molecular polarity, i.e., shorter retention times indicate higher polarity, and longer retention times indicate more nonpolar species. Both (−)HESI and (+)HESI show significant negative correlation between retention and retention time and, therefore, polarity; an F test against the constant-value model shows p values of 0.00193 for (−)HESI and 1.44×10^{-6} for (+)HESI. This indicates that nonpolar species are likely to be unretained, and this appears to be especially true for the previously discussed long-chain species, such as $C_{14}H_{22}$ (m/z 190, 14.5 min, L3) and $C_{15}H_{26}O$ (m/z 222, 14.6 min, L3) compounds. In Fig. 7, a few compound classes can be separated distinctly by polarity, particularly CHOS and CHNO in (−)HESI, as well as CHO and CHNO in (+)HESI. These polarity differences in these classes may be the driving force of the difference in terms of the freezing retention between CHOS and CHNO in (−)HESI, but this is unlikely to be the case for CHO and CHNO in (+)HESI as CHO covers a much wider range of freezing retentions that cannot be explained solely by polarity.

The determined molecular weight (MW) shows little linear correlation with freezing retention (as seen in Fig. S2).

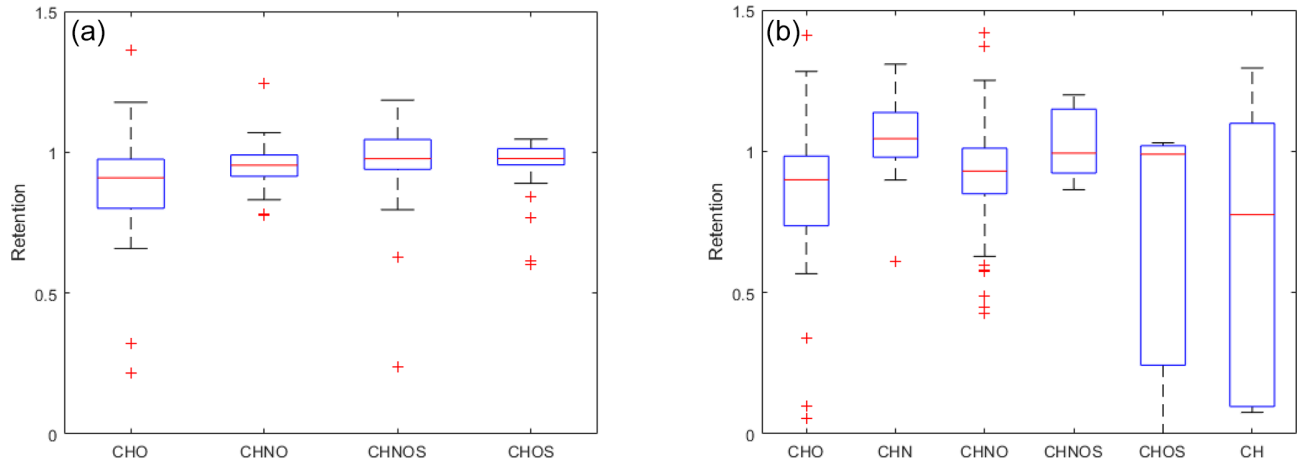

Figure 5. Boxplot of retention coefficients by composition class. **(a)** (−)HESI. **(b)** (+)HESI.

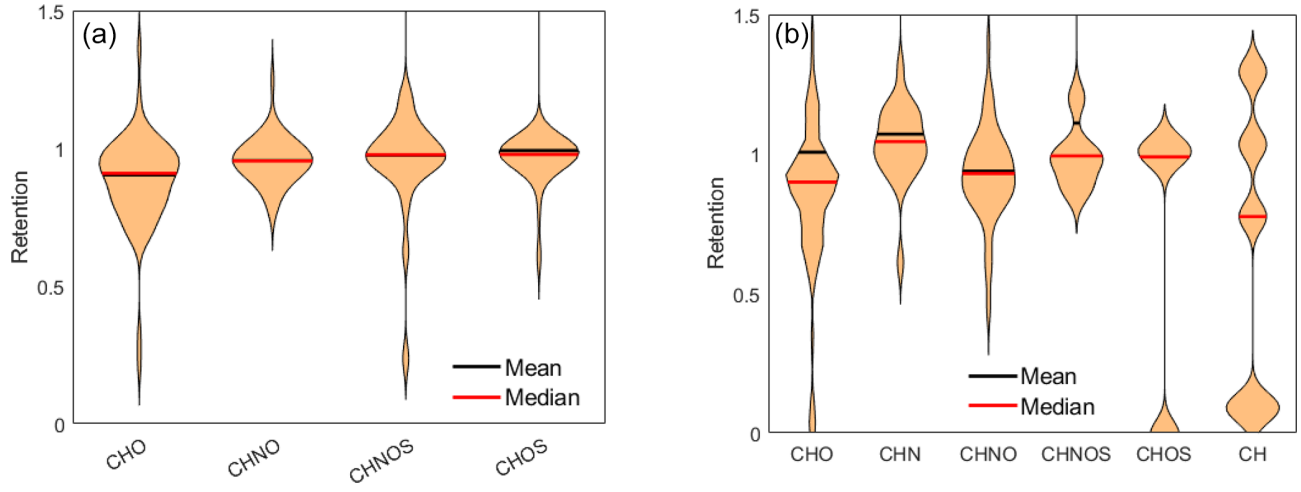

Figure 6. Violin plots of retention coefficients by composition class. **(a)** (−)HESI. **(b)** (+)HESI.

In (−)HESI, the slope of the regression is weakly positive, suggesting that larger compounds are more likely to be retained. This is likely to be related to lower vapor pressures associated with larger MW species in the negative mode. An F test against the constant-value model indicates that this correlation is not significant (p value: 0.0857). However, in (+)HESI, the slope of the regression is weakly negative for MW, which suggests the opposite. An F test against the constant-value model indicates that this correlation with MW is also not significant (p value: 0.1440). This trend in the positive mode is likely to be driven more by polarity as Fig. 1a also demonstrates that larger species in (+)HESI tend to have higher HPLC retention times and are therefore more nonpolar. The plot in Fig. 7 further demonstrates this, with a stronger negative correlation between the HPLC retention time and the freezing retention.

Further chemical property linear regressions with freezing retention could be made for the species with estimated chemical properties. The first plot, shown in Fig. 8, uses the measured retention coefficient to plot against calculated vapor pressure (VP). It demonstrates a significant negative correlation with VP; an F test against the constant-value model gives a p value of 1.42×10^{-4}. It is relevant to note that the majority of species measured are considered to be semi-volatile (vapor pressure: 10^{-9} to 10 Pa; SVOCs) with a few low-volatility (LVOCs) and intermediate-volatility organic compounds (IVOCs) (Li et al., 2023; Manavi and Pandis, 2024). The sampling method is biased against LVOCs and IVOCs, as many LVOCs are highly oxygenated compounds which may be less sensitive compared to other compounds in the UHPLC-Orbitrap MS (Wang et al., 2024), and most IVOCs are revolatilized during sampling (Bidleman et al., 2020). VP is also the property most associated with desorption effects, likely contributing to some of the negative trend seen in Fig. 8. However, it is mostly associated with IVOCs

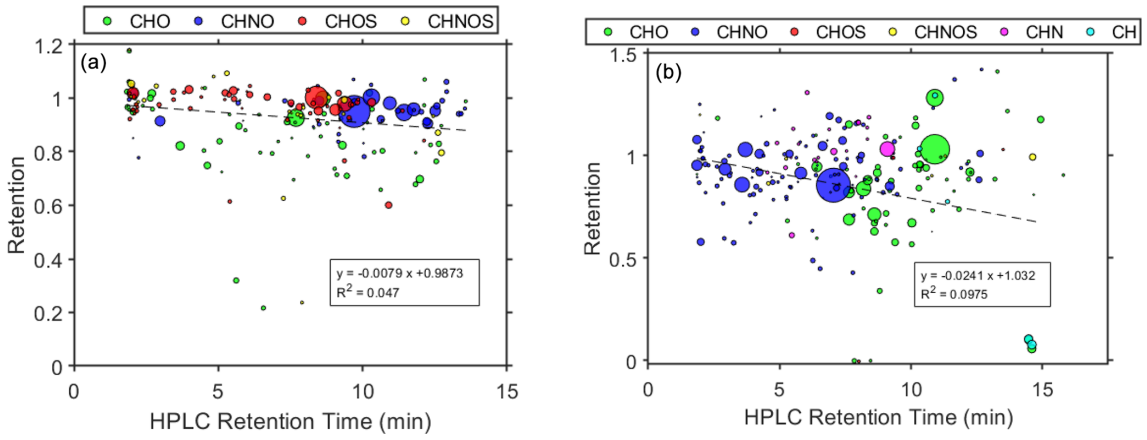

Figure 7. Retention coefficient as a function of HPLC retention time. **(a)** (−)HESI. **(b)** (+)HESI. Color denotes the compositional class of the assigned compound, as used in Fig. 1: green for CHO, blue for CHNO, red for CHOS, yellow for CHNOS, magenta for CHN, and cyan for CH. Dashed line shows linear fit.

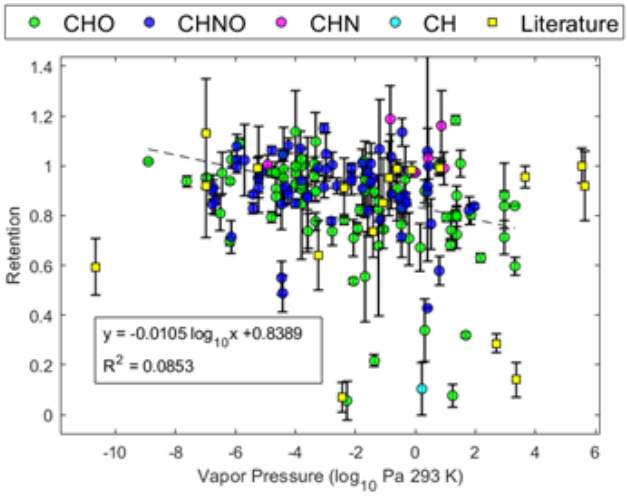

Figure 8. Retention coefficient as a function of estimated vapor pressure. Color denotes the compositional class of the assigned compound: green for CHO, blue for CHNO, magenta for CHN, cyan for CH, and yellow squares for values taken from the literature. Dashed line shows linear fit.

and less with SVOCs, and so desorption alone is not likely to fully explain this correlation.

Demonstrated in Fig. 9, freezing retention shows little or no dependency on H^* under the present experimental conditions. The linear regressions are not significant for either (−)HESI or (+)HESI, with p values of 0.9270 and 0.3530, respectively, for the F test against the constant-value model. The very slight positive slope of the linear regression shows agreement with Stuart and Jacobson's (2003, 2004) observation that high-H^* species are more likely to be 100 % retained, but it does not show sigmoidal behavior as modeled by Jost et al. (2017) (plotted for reference in Fig. 10). This could be the result of differing physical experimental parameters, such as larger droplet sizes (2 mm versus 20 µm). However, directly comparing the known literature values for retention coefficients with the observations made here does not immediately indicate that the systems are incompatible or exclude the comparison.

Figure 10 compares the data presented in Fig. 9 against the literature values presented by Borchers et al. (2024), Jost et al. (2017), and von Blohn et al. (2011, 2013). This comparison does not appear to be incongruous; i.e., no discernible difference can be seen between wind tunnel experiments and these observations. While the measurements presented by Borchers et al. (2024), Jost et al. (2017), and von Blohn et al. (2011, 2013) are physically dissimilar experiments compared to this study – i.e., wind tunnel experiments, small droplets of micrometer size, high-ventilation conditions – their observations are congruent with this experiment. Additionally, there are chemical dissimilarities in these experiments as the present experiment is potentially influenced by activity differences resulting from the extract solution's complexity as opposed to the single- or few-component solutions used by the previously stated studies. Further, the species studied in the current literature are mostly inorganics which are very different in terms of solubility, polarity, and molecular size compared to the organics studied here, i.e., generally more soluble, more polar, and smaller. This could suggest that the organics measured here should have lower retentions than the inorganics in the literature, but that is not observed in the data. However, two of the same nitrophenols studied by Borchers et al. (2024) are measured here: 4-nitrophenol and 2,4-dinitrophenol. It is also likely that 2-nitrobenzoic acid and 4-nitrocatechol or similar analogues are observed within the dataset since other nitro-aromatics that cannot be structurally resolved are observed. Additionally, 2-nitrophenol is also potentially observed; however 2- and 4-nitrophenol are difficult to distinguish from each other as structural isomers and 2-nitrophenol are not easily ionizable in this method.

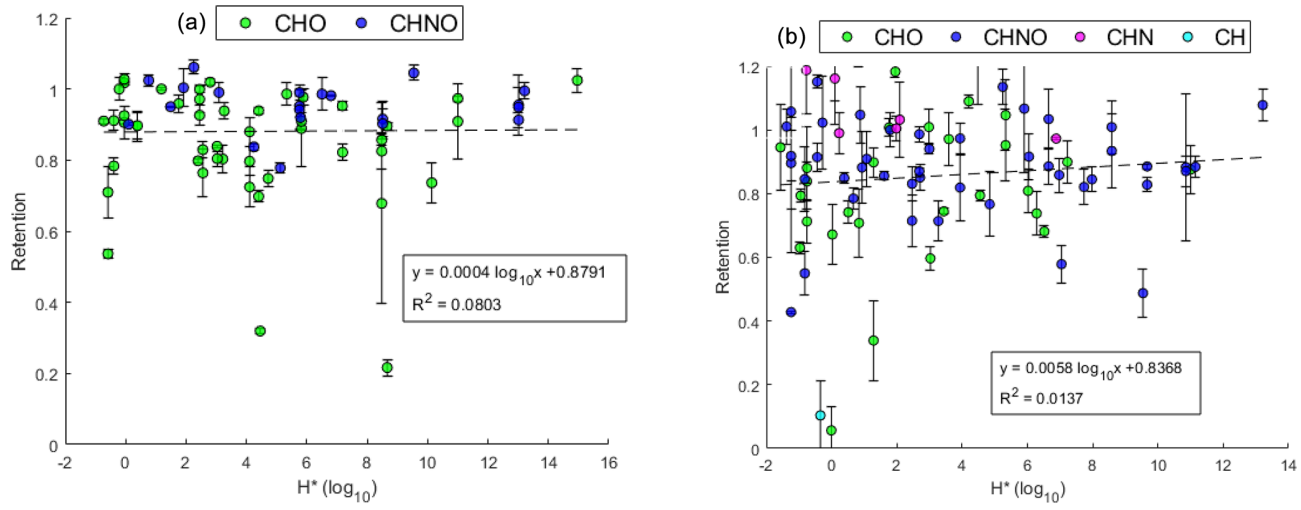

Figure 9. Effective Henry's law constant H^* versus retention coefficient. **(a)** (−)HESI. **(b)** (+)HESI. Color denotes the compositional class of the assigned compound: green for CHO, blue for CHNO, magenta for CHN, and cyan for CH. Dashed line shows linear fit.

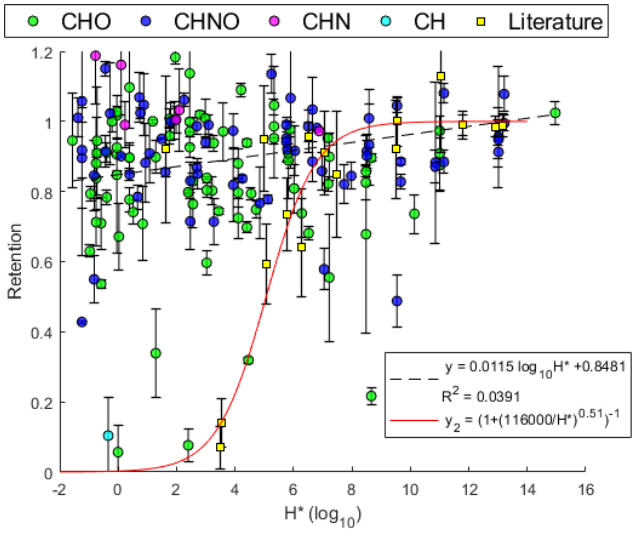

Figure 10. Effective Henry's law constant H^* versus retention coefficient. Color denotes the compositional class of the assigned compound: green for CHO, blue for CHNO, magenta for CHN, and cyan for CH. Yellow squares denote values taken from Borchers et al. (2024), Jost et al. (2017), and von Blohn et al. (2011, 2013). Dashed line shows linear fit. Solid red line gives the parameterization by Jost et al. (2017).

However, these assignments cannot be confirmed without better structural information. The literature values include only three species with $H^* < 10^4$, and two of them, pinanediol and formaldehyde, are excluded from the parameterization presented by Borchers et al. (2024) as they were perceived as outliers. Without more measurements of compounds with $H^* < 10^4$ under wind tunnel conditions, it is difficult to determine if the non-sigmoidal behavior seen in this experiment is the result of different physical parameters – specifically the lower surface-to-volume ratio – or if the sigmoidal behavior described by Borchers et al. (2024) and Jost et al. (2017) is a fit of a limited dataset. Physical differences such as a higher surface-to-volume ratio, increased ventilation, or longer freezing times may result in lower retentions that may primarily affect species with lower H^*, as noted by Jost et al. (2017). Small riming droplets have freezing times in the tens of milliseconds, while the drops here take approximately 90 s to fully freeze. However, the ice shell formation observed by Gautam et al. (2025) in Part 1 is quite fast, in the range of 5 ms. Specifically, these differences either enhance heat and mass transfer, which produces a shorter timescale for expulsion, or increase freezing time, which allows for a wider range of expulsion timescales. Specifically, these differences either enhance heat and mass transfer or provide a longer timescale for expulsion to occur. Describing this in the context of Stuart and Jacobson's (2003, 2004) model, species with larger H^* are more likely to be unaffected by these differences as the gas-phase mass transport term and the interfacial mass transport term are still dominated by H^* despite the decrease in spread droplet height and the increase in thermal velocity, such that the total expulsion time is still much longer than the freezing time. Evidence presented by Gautam et al. (2025) in Part 1 of this publication series makes a compelling case for the dominance of physical parameters at these drop sizes. Critical to these experiments, Gautam et al. (2025) observed the formation of an ice shell, which inhibited any further expulsion of dissolved substances during freezing.

4 Conclusions

This study presents the measurement of the retention coefficients for real, complex WSOCs from urban particulate matter for direct drop freezing under raindrop-sized conditions. The overall distribution of the retention of WSOCs forms a real, non-normal distribution up to 1. Looking at the individual compound classes of organics, the data show that they may have different distributions of retention coefficients. Most negatively ionizable CHNO and CHOS compounds appear to be fully retained, indicating that nitro-aromatics and organosulfates are favorable to be retained. Weak positive correlations between MW, polarity, and H^* are seen with retention, along with a negative correlation with vapor pressure (VP). No sigmoidal relationship with H^* was observed. This is likely to be the result of the lower surface-to-volume ratio for this drop size and the ice shell formation observed by Gautam et al. (2025) in Part 1 of this publication series. However, without further measurements of single-component solutions for compounds with $H^* < 10^4$ under wind tunnel conditions, specifically for small cloud droplet sizes, it is difficult to determine if the non-sigmoidal behavior seen in this experiment is solely the result of physical parameters or if the sigmoidal behavior described by other studies is an overfit of a limited dataset.

The observed sulfides, lipids, aromatic hydrocarbons, and long-chain compounds are among the most unretained and, incidentally, are the fewest species observed. These are also among the most nonpolar species observed, which is presumably the dominant factor in this regard. CHO species show the highest variability in terms of their measured retentions, most likely related to the distributions of polarity and VPs among the sugars, organic acids, and terpenoids seen here.

Aliphatic amines (AAs) do not follow the trends associated with polarity and VP but are among the most highly retained species. The explanation for this is possibly in their structural properties, which cannot be easily determined using this analytical method. AA solubility in water is largely determined by the dimension and structure of the alkyl substituents, such that AAs with longer chains are less soluble than AAs with shorter chains, and AAs with branched substituents are less soluble than AAs with linear groups with the same number of carbons (Badocco et al., 2015). Polarity and hydrogen bonding are also known contributors to AA solubility, but this is not unique to AAs. Indeed, solubility as a property relevant to retention is applicable to all compounds, specifically in how aqueous solubility is related to H^*. While aqueous solubility is a piece of the typical bond method calculation to estimate H^*, it does not necessarily correlate with true H^*. Further analysis on solubility as a factor for retention would be valuable, but the limitations on high-confidence structural assignment in this method prevent its thorough investigation. Structure assignment could also elucidate other retention-relevant properties such as hydrogen-bonding potential or even acid or base effects. Hydrogen-bonding potential may enhance retention along oxygen functionalities, such as among nitro and sulfate species. Hydrogen bonding alone, however, is unlikely to fully explain the high retentions among nitro and sulfate species. Specifically, nitro species have weak hydrogen-bonding potential (Shugrue et al., 2016) and, as a result, are likely to be influenced mostly by the increased polarity imparted by the nitro substituent or its dissociation.

The data suggest that functional groups containing sulfur or nitrogen generally increase a species' ability to be retained. Overall, the high retentions of the nitro and sulfate species typically anthropogenically related to NO_x and SO_2 chemistry indicate that NO_x and SO_2 chemistry may enhance the retention of these SOA species, reducing their likelihood of reaching the upper atmosphere. Furthermore, on this, other studies have demonstrated that NO_x participates in the reversible and irreversible uptake of isoprene to aerosol liquid water and can further react with isoprene to produce a substantial number of organonitrates (El-Sayed et al., 2018; Tsiligiannis et al., 2022). These findings may also indicate that this NO_x chemistry on CHO species enhances their retention in hydrometeors, potentially by increasing its polarity or solubility. Other UHRMS studies of rainwater have suggested similar explanations for nitrogen uptake in hydrometeors and for rainwater organic nitrogen's high bioavailability (Seymore et al., 2023). Additionally, correlations with VP and polarity show that lower-VP species and more polar species tend to be retained. Atmospheric chemical processing generally tends to functionalize or oxidatively degrade large nonpolar species into more water-soluble, less volatile species (Seinfeld and Pandis, 2019). Specifically, aqueous-phase droplet chemistry is known to facilitate condensed-phase SOA formation from highly volatile species (McNeill, 2015). However, many freshly aged terpene products increase in volatility or see only small decreases in VP with oxidation for their early-generation products (Bilde and Pandis, 2001; Kurtén et al., 2018; Wu et al., 2021). This indicates that many freshly oxidized organics may have a lower potential to be retained than aged organics and may generally suggest that freshly oxidized organics are more likely to reach the upper atmosphere than primary organics or aged organics.

The use of UHPLC-HRMS allowed for the study of ambient WSOC retention rather than single-component or limited-mixture experiments from previous studies. While the influence on retention due to activity differences resulting from matrix effects and solution complexity is still unknown, the experiment in this paper demonstrates the viability of UHPLC-HRMS analysis for ambient WSOCs and shows the need for further complex-mixture studies regarding retention. Future studies on retention within hydrometeors should include complex-mixture analysis under the physical conditions most similar to the atmosphere, i.e., wind tunnel experiments, smaller droplets, increased ventilation. As this experiment is a first demonstration of retention within a complex

mixture, the applicability of the conclusions reached here to other locations or samplings with different aerosol compositions – thereby, potentially different matrix effects – could be challenged. For example, black-carbon particles suspended in a drop could strongly bind organic compounds, preventing their transition into the gas phase during freezing; certain surfactant species could change the surface accommodation, inhibiting exchange; or different amounts of inorganic ions could change the ionic strength of the aqueous phase, altering chemical potential. There is not enough evidence to assume that these matrix effects are either negligible or the same elsewhere as in this experiment, but the assumption is not unreasonable. Rainwater tends to show negligible matrix effects for other properties and analyses (Pang et al., 2017; Sauret-Szczepanski et al., 2006). Average rainwater DOC is on the order of µM, which could be assumed to be diluted enough for activity differences to be negligible compared to pure-water solutions. However, these are still unsupported assumptions that are required for broad application of these conclusions. Additionally, broader application of these conclusions should consider the differences in relevant WSOC composition with regard to seasons. This sample set is representative of winter aerosols, which show a high contribution from nitroaromatic compounds, as well as a lower degree of oxidation and a lower proportion of organosulfates in comparison to the summer (Ma et al., 2022). It is also important to note that large-scale convective cloud formation where freezing retention is expected is not typical during the winter, such as when the aerosols in the present study were sampled. Furthermore, in winter, frequent inversion and a low mixing-layer height tend to prevent surface emissions from being transported to higher altitudes and participating in ice cloud formation, and so the compounds presented here may not be wholly representative of the most relevant species that participate in the retention process. Further studies would also be improved with more distinguishable tracers with known retentions and more sophisticated corrections for desorption. Further studies on single-component solutions of species with $H^* < 10^4$ under atmospherically similar physical conditions would also allow for stronger conclusions from the comparison of the retentions measured in this study with other experiments performed under wind tunnel conditions.

The experiment presented here also cannot distinguish between species incorporated within ice crystal structures and those phase-separated but physically constrained to the hydrometeor, potentially between crystal grain boundaries or on the particle surface. This distinction is also not atmospherically relevant with regard to the net transport of organics into the upper troposphere. While this method aims to demonstrate the retention for real WSOCs, this method is still biased against higher volatility species and likely features other sampling biases typical for HiVol-filter-based measurements such as filter extraction bias and solvation effects. These parameterizations of retention also present the distribution of retention coefficients for the variety of species present and not necessarily the mass distribution of species potentially present in the atmosphere. Corrections for species abundance must first be made in order to apply the frequency distribution of the retention coefficients to organic transport models.

Data availability. Data are available at https://doi.org/10.5281/zenodo.15166745 (Seymore, 2025).

Supplement. The supplement related to this article is available online at https://doi.org/10.5194/acp-25-11829-2025-supplement.

Author contributions. JS, MG, MS, and AT participated in designing the experiments. LZ provided the samples. JS and JM prepared the samples for the experiments. MG performed the experiments. JS, JM, and ALV conducted the analytical measurements. JS analyzed the data and wrote the paper draft. MG, MS, AT, JM, ALV, and TH reviewed and edited the paper.

Competing interests. The contact author has declared that none of the authors has any competing interests.

Disclaimer. Publisher's note: Copernicus Publications remains neutral with regard to jurisdictional claims made in the text, published maps, institutional affiliations, or any other geographical representation in this paper. While Copernicus Publications makes every effort to include appropriate place names, the final responsibility lies with the authors.

Special issue statement. This article is part of the special issue "The tropopause region in a changing atmosphere (TPChange) (ACP/AMT/GMD/WCD inter-journal SI)'. It is not associated with a conference.

Acknowledgements. Special thanks are given to Konstantin Dörholt for his initial work and experimentation in the Mainz Wind Tunnel using these samples.

Financial support. This research has been supported by the Deutsche Forschungsgemeinschaft (grant no. TRR 301 – Project-ID 428312742).

This open-access publication was funded by Johannes Gutenberg University Mainz.

Review statement. This paper was edited by Barbara Ervens and reviewed by Amy L. Stuart and two anonymous referees.

References

Andreae, M. O., Afchine, A., Albrecht, R., Holanda, B. A., Artaxo, P., Barbosa, H. M. J., Borrmann, S., Cecchini, M. A., Costa, A., Dollner, M., Fütterer, D., Järvinen, E., Jurkat, T., Klimach, T., Konemann, T., Knote, C., Krämer, M., Krisna, T., Machado, L. A. T., Mertes, S., Minikin, A., Pöhlker, C., Pöhlker, M. L., Pöschl, U., Rosenfeld, D., Sauer, D., Schlager, H., Schnaiter, M., Schneider, J., Schulz, C., Spanu, A., Sperling, V. B., Voigt, C., Walser, A., Wang, J., Weinzierl, B., Wendisch, M., and Ziereis, H.: Aerosol characteristics and particle production in the upper troposphere over the Amazon Basin, Atmos. Chem. Phys., 18, 921–961, https://doi.org/10.5194/acp-18-921-2018, 2018.

Badocco, D., Di Marco, V., Mondin, A., and Pastore, P.: Cyclic voltammetry as a new approach for the determination of solubility of aliphatic amines in water, J. Chem. Eng. Data, 60, 895–901, https://doi.org/10.1021/je5009735, 2015.

Bardakov, R., Thornton, J. A., Riipinen, I., Krejci, R., and Ekman, A. M. L.: Transport and chemistry of isoprene and its oxidation products in deep convective clouds, Tellus B, 73, 1–21, https://doi.org/10.1080/16000889.2021.1979856, 2021.

Bela, M. M., Barth, M. C., Toon, O. B., Fried, A., Ziegler, C., Cummings, K. A., Li, Y., Pickering, K. E., Homeyer, C. R., Morrison, H., Yang, Q., Mecikalski, R. M., Carey, L., Biggerstaff, M. I., Betten, D. P., and Alford, A. A.: Effects of Scavenging, Entrainment, and Aqueous Chemistry on Peroxides and Formaldehyde in Deep Convective Outflow Over the Central and Southeast United States, J. Geophys. Res.-Atmos., 123, 7594–7614, https://doi.org/10.1029/2018JD028271, 2018.

Bidleman, T. F., Falconer, R. L., and Harner, T.: Particle/Gas Distribution of Semivolatile Organic Compounds: Field and Laboratory Experiments with Filtration Samplers, in: Gas and Particle Phase Measurements of Atmospheric Organic Compounds, 39–71, https://doi.org/10.1201/9781003078340-4, 2020.

Bilde, M. and Pandis, S. N.: Evaporation rates and vapor pressures of individual aerosol species formed in the atmospheric oxidation of α- and β- pinene, Environ. Sci. Technol., 35, 3344–3349, https://doi.org/10.1021/es001946b, 2001.

Blair, S. L., MacMillan, A. C., Drozd, G. T., Goldstein, A. H., Chu, R. K., Paša-Tolić, L., Shaw, J. B., Tolić, N., Lin, P., Laskin, J., Laskin, A., and Nizkorodov, S. A.: Molecular Characterization of Organosulfur Compounds in Biodiesel and Diesel Fuel Secondary Organic Aerosol, Environ. Sci. Technol., 51, 119–127, https://doi.org/10.1021/ACS.EST.6B03304, 2017.

Borchers, C., Seymore, J., Gautam, M., Dörholt, K., Müller, Y., Arndt, A., Gömmer, L., Ungeheuer, F., Szakáll, M., Borrmann, S., Theis, A., Vogel, A. L., and Hoffmann, T.: Retention of α-pinene oxidation products and nitro-aromatic compounds during riming, Atmos. Chem. Phys., 24, 13961–13974, https://doi.org/10.5194/acp-24-13961-2024, 2024.

Casquero-Vera, J. A., Lyamani, H., Dada, L., Hakala, S., Paasonen, P., Román, R., Fraile, R., Petäjä, T., Olmo-Reyes, F. J., and Alados-Arboledas, L.: New particle formation at urban and high-altitude remote sites in the south-eastern Iberian Peninsula, Atmos. Chem. Phys., 20, 14253–14271, https://doi.org/10.5194/acp-20-14253-2020, 2020.

Clarke, A. D., Varner, J. L., Eisele, F., Mauldin, R. L., Tanner, D., and Litchy, M.: Particle production in the remote marine atmosphere: Cloud outflow and subsidence during ACE 1, J. Geophys. Res.-Atmos., 103, 16397–16409, https://doi.org/10.1029/97JD02987, 1998.

Clarke, A. D., Eisele, F., Kapustin, V. N., Moore, K., Tanner, D., Mauldin, L., Litchy, M., Lienert, B., Carroll, M. A., and Albercook, G.: Nucleation in the equatorial free troposphere: Favorable environments during PEM-Tropics, J. Geophys. Res.-Atmos., 104, 5735–5744, https://doi.org/10.1029/98JD02303, 1999.

Compernolle, S. and Müller, J.-F.: Henry's law constants of polyols, Atmos. Chem. Phys., 14, 12815–12837, https://doi.org/10.5194/acp-14-12815-2014, 2014.

Diehl, K., Debertshäuser, M., Eppers, O., Schmithüsen, H., Mitra, S. K., and Borrmann, S.: Particle surface area dependence of mineral dust in immersion freezing mode: investigations with freely suspended drops in an acoustic levitator and a vertical wind tunnel, Atmos. Chem. Phys., 14, 12343–12355, https://doi.org/10.5194/acp-14-12343-2014, 2014.

Dusek, U., Frank, G. P., Hildebrandt, L., Curtius, J., Schneider, J., Walter, S., Chand, D., Drewnick, F., Hings, S., Jung, D., Borrmann, S., and Andreae, M. O.: Size matters more than chemistry for cloud-nucleating ability of aerosol particles, Science, 312, 1375–1378, https://doi.org/10.1126/SCIENCE.1125261, 2006.

El-Sayed, M. M. H., Ortiz-Montalvo, D. L., and Hennigan, C. J.: The effects of isoprene and NO_x on secondary organic aerosols formed through reversible and irreversible uptake to aerosol water, Atmos. Chem. Phys., 18, 1171–1184, https://doi.org/10.5194/acp-18-1171-2018, 2018.

Fofie, E. A., Donahue, N. M., and Asa-Awuku, A.: Cloud condensation nuclei activity and droplet formation of primary and secondary organic aerosol mixtures, Aerosol Sci. Technol., 52, 242–251, https://doi.org/10.1080/02786826.2017.1392480, 2018.

Gautam, M., Theis, A., Seymore, J., Hey, M., Borrmann, S., Diehl, K., Mitra, S. K., and Szakáll, M.: Retention during freezing of raindrops – Part 1: Investigation of single and binary mixtures of nitric, formic, and acetic acids and 2-nitrophenol, Atmos. Chem. Phys., 25, 11813–11828, https://doi.org/10.5194/acp-25-11813-2025, 2025.

Hallquist, M., Wenger, J. C., Baltensperger, U., Rudich, Y., Simpson, D., Claeys, M., Dommen, J., Donahue, N. M., George, C., Goldstein, A. H., Hamilton, J. F., Herrmann, H., Hoffmann, T., Iinuma, Y., Jang, M., Jenkin, M. E., Jimenez, J. L., Kiendler-Scharr, A., Maenhaut, W., McFiggans, G., Mentel, Th. F., Monod, A., Prévôt, A. S. H., Seinfeld, J. H., Surratt, J. D., Szmigielski, R., and Wildt, J.: The formation, properties and impact of secondary organic aerosol: current and emerging issues, Atmos. Chem. Phys., 9, 5155–5236, https://doi.org/10.5194/acp-9-5155-2009, 2009.

Heitto, A., Wu, C., Aliaga, D., Blacutt, L., Chen, X., Gramlich, Y., Heikkinen, L., Huang, W., Krejci, R., Laj, P., Moreno, I., Sellegri, K., Velarde, F., Weinhold, K., Wiedensohler, A., Zha, Q., Bianchi, F., Andrade, M., Lehtinen, K. E. J., Mohr, C., and Yli-Juuti, T.: Analysis of atmospheric particle growth based on vapor concentrations measured at the high-altitude GAW station Chacaltaya in the Bolivian Andes, Atmos. Chem. Phys., 24, 1315–1328, https://doi.org/10.5194/acp-24-1315-2024, 2024.

Iinuma, Y., Müller, C., Berndt, T., Böge, O., Claeys, M., and Herrmann, H.: Evidence for the existence of organosulfates from β-pinene ozonolysis in ambient secondary

organic aerosol, Environ. Sci. Technol., 41, 6678–6683, https://doi.org/10.1021/ES070938T, 2007.

Iribarne, J. V. and Pyshnov, T.: The effect of freezing on the composition of supercooled droplets – I. Retention of HCl, HNO_3, NH_3 and H_2O_2, Atmos. Environ. A, 24, 383–387, https://doi.org/10.1016/0960-1686(90)90118-7, 1990.

Isaacman-VanWertz, G. and Aumont, B.: Impact of organic molecular structure on the estimation of atmospherically relevant physicochemical parameters, Atmos. Chem. Phys., 21, 6541–6563, https://doi.org/10.5194/acp-21-6541-2021, 2021.

Jost, A., Szakáll, M., Diehl, K., Mitra, S. K., and Borrmann, S.: Chemistry of riming: the retention of organic and inorganic atmospheric trace constituents, Atmos. Chem. Phys., 17, 9717–9732, https://doi.org/10.5194/acp-17-9717-2017, 2017.

Kaufmann, A. and Walker, S.: Comparison of linear intrascan and interscan dynamic ranges of Orbitrap and ion-mobility time-of-flight mass spectrometers, Rapid Commun. Mass Sp., 31, 1915–1926, https://doi.org/10.1002/RCM.7981, 2017.

Kurtén, T., Hyttinen, N., D'Ambro, E. L., Thornton, J., and Prisle, N. L.: Estimating the saturation vapor pressures of isoprene oxidation products $C_5H_{12}O_6$ and $C_5H_{10}O_6$ using COSMO-RS, Atmos. Chem. Phys., 18, 17589–17600, https://doi.org/10.5194/acp-18-17589-2018, 2018.

Lamb, D. and Verlinde, J.: Physics and Chemistry of Clouds, Cambridge University Press, 275–414, https://doi.org/10.1017/CBO9780511976377, 2011.

Li, J., Gao, X., He, Y., Wang, L., Wang, Y., and Zeng, L.: Elevated emissions of melamine and its derivatives in the indoor environments of typical e-waste recycling facilities and adjacent communities and implications for human exposure, J. Hazard Mater., 432, https://doi.org/10.1016/J.JHAZMAT.2022.128652, 2022.

Li, Y., Pöschl, U., and Shiraiwa, M.: Molecular corridors and parameterizations of volatility in the chemical evolution of organic aerosols, Atmos. Chem. Phys., 16, 3327–3344, https://doi.org/10.5194/acp-16-3327-2016, 2016.

Li, Z., Hyttinen, N., Vainikka, M., Tikkasalo, O.-P., Schobesberger, S., and Yli-Juuti, T.: Saturation vapor pressure characterization of selected low-volatility organic compounds using a residence time chamber, Atmos. Chem. Phys., 23, 6863–6877, https://doi.org/10.5194/acp-23-6863-2023, 2023.

Liu, J., Zhang, F., Xu, W., Sun, Y., Chen, L., Li, S., Ren, J., Hu, B., Wu, H., and Zhang, R.: Hygroscopicity of Organic Aerosols Linked to Formation Mechanisms, Geophys. Res. Lett., 48, e2020GL091683, https://doi.org/10.1029/2020GL091683, 2021.

Liu, Z., Yim, S. H. L., Wang, C., and Lau, N. C.: The Impact of the Aerosol Direct Radiative Forcing on Deep Convection and Air Quality in the Pearl River Delta Region, Geophys. Res. Lett., 45, 4410–4418, https://doi.org/10.1029/2018GL077517, 2018.

Ma, J., Ungeheuer, F., Zheng, F., Du, W., Wang, Y., Cai, J., Zhou, Y., Yan, C., Liu, Y., Kulmala, M., Daellenbach, K. R., and Vogel, A. L.: Nontarget Screening Exhibits a Seasonal Cycle of $PM_{2.5}$ Organic Aerosol Composition in Beijing, Environ. Sci. Technol., 56, 7017–7028, https://doi.org/10.1021/acs.est.1c06905, 2022.

Manavi, S. E. I. and Pandis, S. N.: Contribution of intermediate-volatility organic compounds from on-road transport to secondary organic aerosol levels in Europe, Atmos. Chem. Phys., 24, 891–909, https://doi.org/10.5194/acp-24-891-2024, 2024.

McNeill, V. F.: Aqueous organic chemistry in the atmosphere: Sources and chemical processing of organic aerosols, Environ. Sci. Technol., 49, 1237–1244, https://doi.org/10.1021/es5043707, 2015.

Nolan, J. P.: Univariate Stable Distributions, Springer Nature Link, https://doi.org/10.1007/978-3-030-52915-4, 2020.

Pang, X., Lewis, A. C., and Shaw, M. D.: Analysis of biogenic carbonyl compounds in rainwater by stir bar sorptive extraction technique with chemical derivatization and gas chromatography-mass spectrometry, J. Sep. Sci., 40, 753–766, https://doi.org/10.1002/JSSC.201600561, 2017.

Pruppacher, H. R. and Klett, J. D.: Microphysics of Clouds and Precipitation, 18, https://doi.org/10.1007/978-0-306-48100-0, 2010.

Price, D. J., Clark, C. H., Tang, X., Cocker, D. R., Purvis-Roberts, K. L., and Silva, P. J.: Proposed chemical mechanisms leading to secondary organic aerosol in the reactions of aliphatic amines with hydroxyl and nitrate radicals, Atmos. Environ., 96, 135–144, https://doi.org/10.1016/J.ATMOSENV.2014.07.035, 2014.

Price, D. J., Kacarab, M., Cocker, D. R., Purvis-Roberts, K. L., and Silva, P. J.: Effects of temperature on the formation of secondary organic aerosol from amine precursors, Aerosol Sci. Technol., 50, 1216–1226, https://doi.org/10.1080/02786826.2016.1236182, 2016.

Qi, L., Zhang, Z., Wang, X., Deng, F., Zhao, J., and Liu, H.: Molecular characterization of atmospheric particulate organosulfates in a port environment using ultrahigh resolution mass spectrometry: Identification of traffic emissions, J. Hazard Mater., 419, 126431, https://doi.org/10.1016/J.JHAZMAT.2021.126431, 2021.

Qian, K., Kumar, A., Patil, K., Bellmer, D., Wang, D., Yuan, W., and Huhnke, R. L.: Effects of Biomass Feedstocks and Gasification Conditions on the Physiochemical Properties of Char, Energies, 6, 3972–3986, https://doi.org/10.3390/EN6083972, 2013.

Riva, M., Chen, Y., Zhang, Y., Lei, Z., Olson, N., Chelmo, H. B., Narayan, S., Yee, L., Green, H., Cui, T., Zhang, Z., Baumann, K., Fort, M., Edgerton, E., Budisulistiorini, S., Rose, C., Ribeiro, I., Oliveira, R. e, Santos, E. dos, Machado, C., Szopa, S., Zhao, Y., Alves, E., Sá, S. de, Hu, W., Knipping, E., Shaw, S., Junior, S. D., Souza, R. de, Palm, B., Jimenez, J., Glasius, M., Goldstein, A., Pye, H., Gold, A., Turpin, B., Vizuete, W., Martin, S., Thornton, J., Dutcher, C., Ault, A., and Surratt, J.: Increasing Isoprene Epoxydiol-to-Inorganic Sulfate Aerosol Ratio Results in Extensive Conversion of Inorganic Sulfate to Organosulfur Forms: Implications for Aerosol Physicochemical Properties, Environ. Sci. Technol, 53, 8682–8694, https://doi.org/10.1021/acs.est.9b01019, 2019.

Sauret-Szczepanski, N., Mirabel, P., and Wortham, H.: Development of an SPME–GC–MS/MS method for the determination of pesticides in rainwater: Laboratory and field experiments, Environ. Pollut., 139, 133–142, https://doi.org/10.1016/J.ENVPOL.2005.04.024, 2006.

Saxena, P. and Hildemann, L. M.: Water-Soluble Organics in Atmospheric Particles: A Critical Review of the Literature and Application of Thermodynamics to Identify Candidate Compounds, J. Atmos. Chem., 24, 57–109, 1996.

Schollée, J. E., Schymanski, E. L., Stravs, M. A., Gulde, R., Thomaidis, N. S., and Hollender, J.: Similarity of High-Resolution Tandem Mass Spectrometry Spectra of Structurally Related Micropollutants and Transformation Products, J. Am. Soc. Mass. Spectrom., 28, 2692–2704, https://doi.org/10.1007/S13361-017-1797-6, 2017.

Schymanski, E. L., Jeon, J., Gulde, R., Fenner, K., Ruff, M., Singer, H. P., and Hollender, J.: Identifying small molecules via high resolution mass spectrometry: Communicating confidence, Environ. Sci. Technol., 48, 2097–2098, https://doi.org/10.1021/ES5002105, 2014.

Seinfeld, J. H. and Pandis, S. N.: Atmospheric Chemistry and Physics: From Air Pollution to Climate Change, 3rd edn., 1–1152, ISBN 978-1-118-94740-1, 2019.

Seymore, J.: Retention Coefficients Measured from Acoustic Levitator Untargeted Mass Spec Experiments Using Beijing Filter Samples [Data set], Zenodo [data set], https://doi.org/10.5281/zenodo.15166745, 2025.

Seymore, J., Felix, J. D., Abdulla, H., Bergmann, D., Campos, M. L. A. M., and Florêncio, J.: Pandemic-Related Anthropogenic Influences on the Dissolved Organic Matter Chemical Character in São Paulo State Wet Deposition by Ultrahigh-Resolution Mass Spectrometry, ACS Earth Space Chem., 7, 1929–1946, https://doi.org/10.1021/acsearthspacechem.3c00076, 2023.

Shugrue, C. R., Defrancisco, J. R., Metrano, A. J., Brink, B. D., Nomoto, R. S., and Linton, B. R.: Detection of weak hydrogen bonding to fluoro and nitro groups in solution using H/D exchange, Org. Biomol. Chem., 14, 2223–2227, https://doi.org/10.1039/C5OB02360B, 2016.

Snider, J. R. and Huang, J.: Factors influencing the retention of hydrogen peroxide and molecular oxygen in rime ice, J. Geophys. Res. Atmos., 103, 1405–1415, https://doi.org/10.1029/97JD02847, 1998.

Snider, J. R., Montague, D. C., and Vali, G.: Hydrogen peroxide retention in rime ice, J. Geophys. Res.-Atmos., 97, 7569–7578, https://doi.org/10.1029/92JD00237, 1992.

Stuart, A. L. and Jacobson, M. Z.: A timescale investigation of volatile chemical retention during hydrometeor freezing: Nonrime freezing and dry growth riming without spreading, J. Geophys. Res.-Atmos., 108, 4178, https://doi.org/10.1029/2001JD001408, 2003.

Stuart, A. L. and Jacobson, M. Z.: Chemical retention during dry growth riming, J. Geophys. Res.-Atmos., 109, D07305, https://doi.org/10.1029/2003JD004197, 2004.

Sun, H., Li, X., Zhu, C., Huo, Y., Zhu, Z., Wei, Y., Yao, L., Xiao, H., and Chen, J.: Molecular composition and optical property of humic-like substances (HULIS) in winter-time $PM_{2.5}$ in the rural area of North China Plain, Atmos. Environ., 252, 118316, https://doi.org/10.1016/j.atmosenv.2021.118316, 2021.

Surratt, J. D., Kroll, J. H., Kleindienst, T. E., Edney, E. O., Claeys, M., Sorooshian, A., Ng, N. L., Offenberg, J. H., Lewandowski, M., Jaoui, M., Flagan, R. C., and Seinfeld, J. H.: Evidence for organosulfates in secondary organic aerosol, Environ. Sci. Technol., 41, 517–527, https://doi.org/10.1021/ES062081Q, 2007.

Szakáll, M., Debertshäuser, M., Lackner, C. P., Mayer, A., Eppers, O., Diehl, K., Theis, A., Mitra, S. K., and Borrmann, S.: Comparative study on immersion freezing utilizing single-droplet levitation methods, Atmos. Chem. Phys., 21, 3289–3316, https://doi.org/10.5194/acp-21-3289-2021, 2021.

Taneda, S., Mori, Y., Kamata, K., Hayashi, H., Furuta, C., Li, C., Seki, K. I., Sakushima, A., Yoshino, S., Yamaki, K., Watanabe, G., Taya, K., and Suzuki, A. K.: Estrogenic and anti-androgenic activity of nitrophenols in diesel exhaust particles (DEP), Biol. Pharm. Bull., 27, 835–837, https://doi.org/10.1248/BPB.27.835, 2004.

Tsiligiannis, E., Wu, R., Lee, B. H., Salvador, C. M., Priestley, M., Carlsson, P. T. M., Kang, S., Novelli, A., Vereecken, L., Fuchs, H., Mayhew, A. W., Hamilton, J. F., Edwards, P. M., Fry, J. L., Brownwood, B., Brown, S. S., Wild, R. J., Bannan, T. J., Coe, H., Allan, J., Surratt, J. D., Bacak, A., Artaxo, P., Percival, C., Guo, S., Hu, M., Wang, T., Mentel, T. F., Thornton, J. A., and Hallquist, M.: A Four Carbon Organonitrate as a Significant Product of Secondary Isoprene Chemistry, Geophys. Res. Lett., 49, e2021GL097366, https://doi.org/10.1029/2021GL097366, 2022.

US EPA: Caprolactam – EPA Health Effects Notebook for Hazardous Air Pollutants, 2020.

US EPA: EPI Suite™ – Estimation Program Interface, US EPA, https://www.epa.gov/tsca-screening-tools/epi-suitetm-estimation-program-interface#citing, last access: December 2024.

von Blohn, N., Diehl, K., Mitra, S. K., and Borrmann, S.: Wind tunnel experiments on the retention of trace gases during riming: nitric acid, hydrochloric acid, and hydrogen peroxide, Atmos. Chem. Phys., 11, 11569–11579, https://doi.org/10.5194/acp-11-11569-2011, 2011.

von Blohn, N., Diehl, K., Nölscher, A., Jost, A., Mitra, S. K., and Borrmann, S.: The retention of ammonia and sulfur dioxide during riming of ice particles and dendritic snow flakes: Laboratory experiments in the Mainz vertical wind tunnel, J. Atmos. Chem., 70, 131–150, https://doi.org/10.1007/S10874-013-9261-X, 2013.

Wang, K., Zhang, Y., Tong, H., Han, J., Fu, P., Huang, R. J., Zhang, H., and Hoffmann, T.: Molecular-Level Insights into the Relationship between Volatility of Organic Aerosol Constituents and $PM_{2.5}$ Air Pollution Levels: A Study with Ultrahigh-Resolution Mass Spectrometry, Environ. Sci. Technol., 58, 7947–7957, https://doi.org/10.1021/acs.est.3c10662, 2024.

Weigel, R., Borrmann, S., Kazil, J., Minikin, A., Stohl, A., Wilson, J. C., Reeves, J. M., Kunkel, D., de Reus, M., Frey, W., Lovejoy, E. R., Volk, C. M., Viciani, S., D'Amato, F., Schiller, C., Peter, T., Schlager, H., Cairo, F., Law, K. S., Shur, G. N., Belyaev, G. V., and Curtius, J.: In situ observations of new particle formation in the tropical upper troposphere: the role of clouds and the nucleation mechanism, Atmos. Chem. Phys., 11, 9983–10010, https://doi.org/10.5194/acp-11-9983-2011, 2011.

Williamson, C. J., Kupc, A., Axisa, D., Bilsback, K. R., Bui, T. P., Campuzano-Jost, P., Dollner, M., Froyd, K. D., Hodshire, A. L., Jimenez, J. L., Kodros, J. K., Luo, G., Murphy, D. M., Nault, B. A., Ray, E. A., Weinzierl, B., Wilson, J. C., Yu, F., Yu, P., Pierce, J. R., and Brock, C. A.: A large source of cloud condensation nuclei from new particle formation in the tropics, Nature, 574, 399–403, https://doi.org/10.1038/s41586-019-1638-9, 2019.

Wu, R., Vereecken, L., Tsiligiannis, E., Kang, S., Albrecht, S. R., Hantschke, L., Zhao, D., Novelli, A., Fuchs, H., Tillmann, R., Hohaus, T., Carlsson, P. T. M., Shenolikar, J., Bernard, F., Crowley, J. N., Fry, J. L., Brownwood, B., Thornton, J. A., Brown, S. S., Kiendler-Scharr, A., Wahner, A., Hallquist, M., and Mentel, T. F.: Molecular composition and volatility of multi-generation products formed from isoprene oxidation by nitrate radical, Atmos. Chem. Phys., 21, 10799–10824, https://doi.org/10.5194/acp-21-10799-2021, 2021.

Xing, C., Wan, Y., Wang, Q., Kong, S., Huang, X., Ge, X., Xie, M., and Yu, H.: Molecular Characterization of Brown Carbon Chromophores in Atmospherically Relevant Samples and

Their Gas-Particle Distribution and Diurnal Variation in the Atmosphere, J. Geophys. Res.-Atmos., 128, e2022JD038142, https://doi.org/10.1029/2022JD038142, 2023.

Yee, T. W.: Univariate Continuous Distributions, 343–370, https://doi.org/10.1007/978-1-4939-2818-7_12, 2015.

Zhang, Q., Anastasio, C., and Jimenez-Cruz, M.: Water-soluble organic nitrogen in atmospheric fine particles ($PM_{2.5}$) from northern California, J. Geophys. Res.-Atmos., 107, AAC 3-1, https://doi.org/10.1029/2001JD000870, 2002.

Zheng, G., Wang, Y., Wood, R., Jensen, M. P., Kuang, C., McCoy, I. L., Matthews, A., Mei, F., Tomlinson, J. M., Shilling, J. E., Zawadowicz, M. A., Crosbie, E., Moore, R., Ziemba, L., Andreae, M. O., and Wang, J.: New particle formation in the remote marine boundary layer, Nat. Commun., 12, 1–10, https://doi.org/10.1038/s41467-020-20773-1, 2021.